FULL PAPER

Nanospherical Surface-Supported Seeded Growth of Au Nanowires: Investigation on a New Growth Mechanism and High-Performance Hydrogen Peroxide Sensors

Ying Li, Lianhai Zu, Guanglei Liu, Yao Qin, Donglu Shi, and Jinhu Yang**

In this paper, a novel strategy with a new growth mechanism for fast and large-scale growth of Au long nanowires on high-curvature SiO_2 nanospherical surfaces has been developed. The synthesis includes three steps, i.e., amino modification of SiO_2 nanospheres, Au seed loading on aminated SiO_2 nanospheres and subsequently, Au seed-mediated nanowire growth on SiO_2 nanospheres. The prepared Au nanowires (Au NWs) (exhibit long length, high aspect ratio, and good flexibility, and can naturally form the dense nanowire film, which is promising as a stable conductive electrode. In addition, the effect of synthetic conditions such as reactant feeding order, Au seeds and SiO_2@Au seeds on the morphology of Au nanostructures (nanowires, nanoteeth, and nanoflowers) has been investigated. It is found that Au seeds and high-curvature SiO_2 nanospherical surfaces are necessary conditions for the successful preparation of Au NWs and nanowire films. The different growth mechanisms for Au NWs and nanoteeth have been proposed and discussed. Moreover, the novel nonenzymatic H_2O_2 sensor based on Au NWs exhibits much enhanced performance such as higher sensitivity, stability, and selectivity, wider linear range and lower detection limit, compared with that of Au nanoparticles-based H_2O_2 sensor.

1. Introduction

One-dimensional (1D) Au nanomaterials have attracted considerable attention in the past decade due to their special optical and electrical properties, good biocompatibility, and great potentials in biomedicine, catalysis, and sensors.[1–14]

Y. Li, L. H. Zu, G. L. Liu, Prof. J. H. Yang
Department of Chemistry
Tongji University
Siping Road 1239, Shanghai 200092, P. R. China
E-mail: yangjinhu2010@gmail.com
Prof. Y. Qin, Prof. J. H. Yang
Research Center for Translational Medicine and Key
Laboratory of Arrhythmias of the Ministry of Education of China
East Hospital, Tongji University School of Medicine
No. 150 Jimo Road, Shanghai 200120, P. R. China
E-mail: qinyao83@gmail.com
Prof. D. L. Shi
Materials Science and Engineering Program
Department of Mechanical and Materials Engineering
College of Engineering and Applied Science
University of Cincinnati
Cincinnati, OH 45221, USA

As a typical representative of 1D structures, Au nanowires (Au NWs) have a wide application prospect in nanoelectronics/microelectronics, nanodevices, and sensors.[11–14] Various methods have been employed to fabricate Au NWs such as hard template method,[15–17] template-free wet chemical synthesis,[18–21] and so on. Generally speaking, precise control on diameter, length, and assembly of Au NWs can be realized by using hard templates in spite of disadvantages of low yield, high cost, and complicated processes during template synthesis and removal. In contrast, wet chemical synthesis is an important means for the fabrication of Au NWs due to its versatility, low cost, and mild conditions. However, because the wet synthetic system is very complex, Au NWs prepared through different synthetic systems may be associated with different growth mechanism. For example, ultrathin single-crystalline Au NWs were formed via the oriented attachment mechanism by Halder and Ravishankar.[19] Unique Au wavy NWs had been prepared at the air/water interface through attachment and cold welding.[20] Particularly, novel Au NW forests formed on a trumpet shell or flat Si wafer with a new-type seeded growth model that is similar in appearance to classic vapor–liquid–solid (VLS) growth were realized.[21] To date, there still remains great significance and challenge to fully understand the nanowire growth mechanism in aqueous solution.

It is noted that noble metal (Au, Ag, etc) nanowire films are emerging as promising substitutes of conventional conductive substrates in a wide variety of practical devices such as robust flexible electronics[22] and transparent electrodes.[12,13,23,24] In this regards, the facile large-scale preparation of Au NW films with excellent mechanical strength and good conductivity is crucial for practical applications. However, the previous NW synthetic methods are not favorable with respect to this goal. For instance, Au NWs prepared by wet chemical way were usually in the forms of dispersed state that is hard to form stable films. Through the hard template method could produce Au NW films directly, the parallel assembly of nanowires might cause poor interaction between nanowires and low mechanical strength of Au NW films.[16] Therefore, new synthetic strategy for Au NWs and Au NW films with favored property for advanced device construction is highly desired.

On the other hand, H_2O_2 is a byproduct or an intermediate product generated from many fundamental biological oxidative reactions and important industrial processes. It is important to develop simple, rapid, and sensitive methods for H_2O_2 detection. At present, a number of H_2O_2 detection methods have been explored.[25–31] Among them, the electrochemical techniques have attracted much more attention due to their great advantages of low cost, rapid response, simple instrumentation, high sensitivity, and selectivity. Especially, typical peroxidase[32–35] or hemoglobin[36,37]-based enzyme biosensors have been constructed for H_2O_2 measurement. However, their applications have been limited by some disadvantages of enzyme, such as high cost, instability, easy inactivation, and critical demand on the environmental condition. Therefore, many efforts have been made to develop new-type nonenzymatic sensors.

Inspired by the seed-mediated growth of Au NW forest,[21] in this work, we develop a new strategy and extend the synthesis from flat substrate to high-curvature nanospherical surfaces, for fast and large-scale fabrication of long Au NWs and Au NW films. A new different seeded growth mechanism where the active growth frontier at one end of Au NWs was always next to solution, rather than next to substrate in nanowire forest case[21] or Au catalysts in VLS growth,[38–42] has been proposed and discussed. The synthetic strategy for Au NWs includes a three-step approach, i.e., amine modification of SiO_2 nanospheres, Au seed deposition on aminated SiO_2 nanospheres, and seeded growth of Au NWs on the surfaces of SiO_2 nanospheres with the assistance of 4-mercaptobenzoic acid (MBA). The as-prepared Au NWs exhibit long length, high aspect ratio, good flexibility as well as high uniformity, and can naturally form a dense film consisting of interdigitated Au NWs owing to the fast seeded-growth on the surfaces of SiO_2 nanospheres. The H_2O_2 sensors based on the long Au NW film demonstrate enhanced performance, such as higher sensitivity and stability, better selectivity, wider linear range, and lower detection limit, compared with that of Au nanoparticles-based H_2O_2 sensor.

2. Results and Discussion

Figure 1 shows the synthetic route to the fabrication of long Au NWs on SiO_2 nanospheres (SiO_2@Au NWs). Briefly, SiO_2 nanospheres were first modified with amino groups, serving as highly curved substrates for deposition of Au seeds and subsequent growth of Au NWs (Figure 1, step I). Then, citrate-capped Au seeds (8 nm) were deposited firmly on SiO_2 nanospheres

to form stable core–shell SiO_2@Au seed composites, due to the strong electrostatic interactions between positively charged SiO_2 nanospheres and negatively charged Au seeds (Step II). Finally, fast growth of Au NWs on Au seed-loaded SiO_2 nanospheres was occurred in the presence of MBA when $HAuCl_4$ and VC were introduced, leading to the formation of the SiO_2@Au NWs (Step III).

Figure 2A shows scanning electron microscope (SEM) image of SiO_2@Au seed composites. It can be seen that the composites present uniform size and good dispersity, as well as uniform deposition of Au seeds on SiO_2 nanospheres. The average diameters of SiO_2 nanospheres and Au seeds are about 220 and 8 nm, respectively, in agreement with these of pristine SiO_2 nanospheres and freshly prepared Au seeds before the deposition. The long Au NWs growing on SiO_2 nanospheres were obtained after a 15-min fast growth mediated by Au seeds, as shown in SEM images in Figure 2B,C. It appears that each nanowire has a head at the end close to SiO_2 nanospheres. (Figure 2B inset and Figure S1, Supporting Information). The fast radial growth of long Au NWs from SiO_2 nanospheres makes nanowires interdigitated. Consequently, the nanowires can form a dense film after collection through centrifugation (Figure 2B). Interestingly, almost each SiO_2 nanosphere is densely wrapped by Au NWs (inset in Figure 2B,C). This reveals that the growth of Au NWs started from Au seeds of the SiO_2@Au seed composites and confirms an Au seed-mediated growth mechanism. From a magnified SEM image of Figure 2D, several single nanowires with their lengths over 2 μm and diameters of about 5 nm are observed after sonication, giving a high aspect ratio of 400. The corresponding transmission electron microscopy (TEM) characterizations of Au NWs are shown in Figure 2E–G. The nanowires that show curved shape and uniform diameter of 5 nm are still entangled after sonication (Figure 2E). The high-resolution transmission electron microscopy (HRTEM) image of a single nanowire (Figure 2F,G) gives clear crystal lattices with d-spacing of 0.235 nm corresponding to the (111) planes of face-centered cubic (fcc) gold, indicating the nanowires are composed of pure metal Au. This is well consistent with the result of X-ray diffraction (XRD) characterization of the Au NWs (Figure S2, Supporting Information).

The synthesis of the long Au NWs can be scaled up. As shown in Figure S3 (Supporting Information), the long Au NWs are still formed at a high reactant concentration five times that of the typical. The Au NWs prepared at this high concentration also display thin diameter, long length, and high flexibility. Although some Au nanoparticles are coexisted, Au NWs occupy
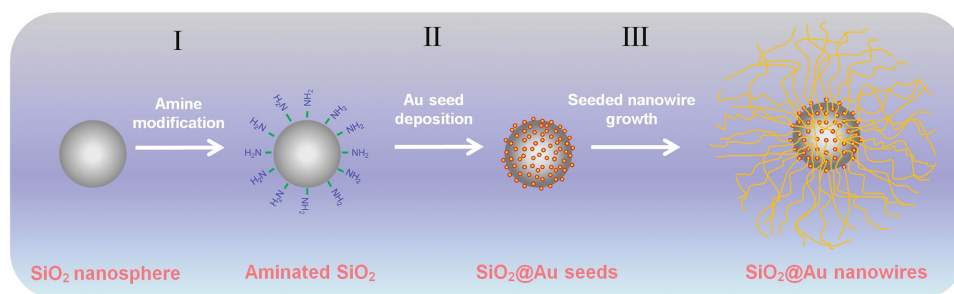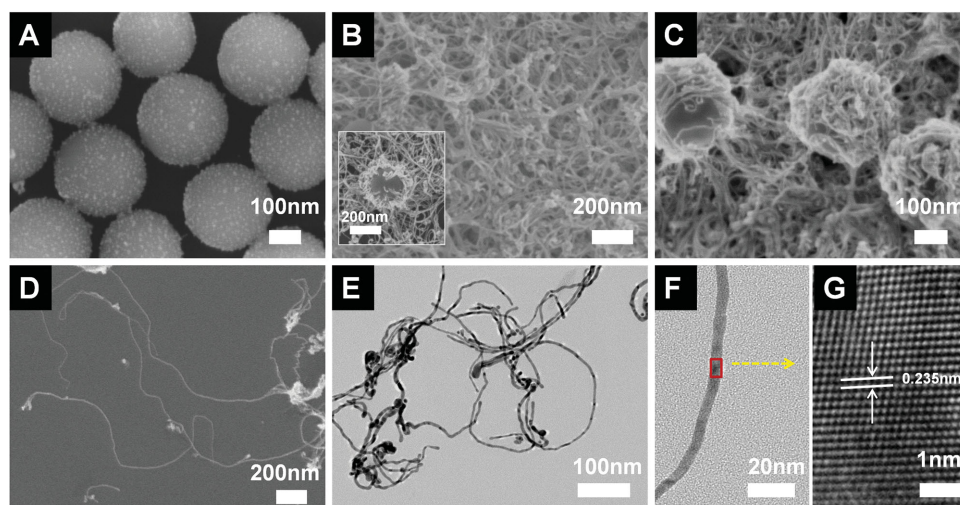

**Figure 1.** Schematic illustration of the synthetic route to the preparation of long Au NWs on SiO_2 nanospheres.

Figure 2. A) SEM image of SiO$_2$@Au seed composites. B–D) SEM images of SiO$_2$@Au NW composites. E–G) TEM and high-resolution TEM images of long Au nanowires.

the majority in the product. We think that the Au nanoparticles are formed through a homogeneous nucleation/growth process in the solution other than seeded growth on Au seeds. Moreover, Au nanoparticles can be removed technically by the filtration method. Therefore, the proposed synthetic strategy is an effective way for the preparation of Au NW on a large scale.

The optical properties of the several different samples including Au seeds, SiO$_2$@Au seeds, Au NWs, and SiO$_2$@Au NWs were investigated, as shown in **Figure 3**. The absorption peaks of the Au seeds, SiO$_2$@Au seeds, SiO$_2$@Au NWs, and Au NWs are centered at 520, 550, 580, and 580 nm, respectively, giving an obvious red shift as indicated by the arrow. The absorption peak shift is obviously caused by the different structural characteristics of Au nanoseeds and nanowires.[9,10] In addition, the absorption band widening of the samples from Au seeds, SiO$_2$@Au seeds to Au NWs is observed, which

is considered to be resulted from the unique surface plasmon resonance (SPR) effect of Au. It was reported that the assembly of Au nanoparticles at a certain density could lead to plasmon resonance coupling and enhanced visible light adsorption.[43–45] Particularly, Au nanoparticles assembled uniformly on the surfaces of SiO$_2$ nanospheres demonstrated novel property of temperature-dependent SPR peak shift, which promise the application as novel thermometers.[45] The absorption spectra difference in visible light bands expresses as different optical colors of the four samples. As can be seen, the color change from red, pink to gray, following the same order of the samples, is also demonstrated (inset in Figure 3), corresponding well to their absorption spectra.

It is found that the feeding order of HAuCl$_4$ and L-ascorbic acid (AA) plays a prominent role in determining both the final structure of SiO$_2$@Au NWs and their growth mechanism. As shown in **Figure 4**A, if the synthesis was conducted by adding HAuCl$_4$ prior to AA under otherwise the same conditions, the novel core–shell composites consisting of Au nanoteeth array on SiO$_2$ nanospheres were formed. A high-magnification SEM image in Figure 4B reveals that the Au nanoteeth were about 50 nm in length, which is much shorter than the length of Au NWs shown in Figure 2B. Interestingly, unlike typical long Au NWs whose wire shape started from the heads (Au seed) (Figure 2B and Figure S1, Supporting Information), the Au nanoteeth seemed to end up with the heads (Figure 4B). The possible mechanism for the formation of Au nanoteeth or nanowires on SiO$_2$ nanospheres by merely changing the feeding order of HAuCl4 and AA has been proposed, as demonstrated in **Figure 5**. In the typical synthesis, when AA was added first into the dispersion solution of the SiO$_2$@Au seed composites, AA molecules were uniformly distributed throughout the solution. This provided the equal opportunity, in theory, for AA molecules to capture HAuCl$_4$ molecules to form Au nuclei both on Au seeds around SiO$_2$ nanospheres and in solution. Nevertheless, the nucleation on Au seeds is much preferable in energy relative to homogeneous nucleation in solution phase.[21] Therefore, the faster nucleation and nanowire growth at sites of Au
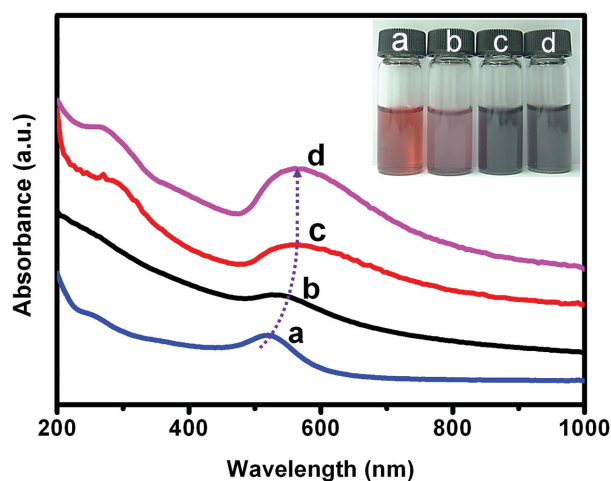
Figure 3. UV-vis-NIR absorption spectra of a) Au seeds, b) SiO$_2$@Au seeds, c) SiO$_2$@Au NWs, d) Au NWs. Inset: photographs of the four samples. The dotted line arrows the gradual red shift of absorption peaks for the four samples.
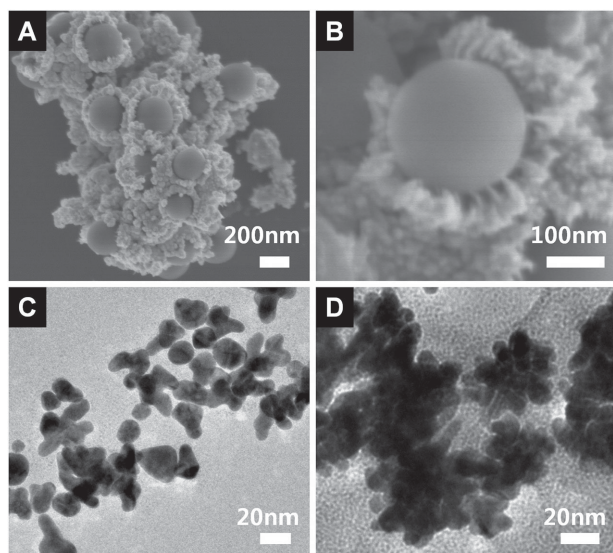
Figure 4. SEM and TEM images of various Au nanostructures prepared under different synthetic conditions. A,B) SiO$_2$@Au nanoteeth synthesized by the feeding order of HAuCl$_4$+AA; C) TEM image of Au nanoparticles synthesized without SiO$_2$@Au seeds; D) TEM image of Au nanoflowers synthesized without SiO$_2$ nanospheres.

seeds were proceeded, leading to rapid depletion of Au sources (such as HAuCl$_4$ and Au nuclei) and producing a concentration gradient of Au nuclei from solution to SiO$_2$ nanospheres. Driven by the concentration gradient, Au nuclei formed in solution were diffused to the growth frontier of primary Au NWs on SiO$_2$ nanospheres, resulting in the long Au NWs after the seeded growth process. In contrast, in the second case, when HAuCl4 was added first, HAuCl$_4$ molecules were prone to be enriched on the surfaces of the SiO$_2$@Au seed composites, due to their strong interactions with mercapto groups from MBA molecules that were covalently modified to Au seeds. The enrichment gave rise to a higher local concentration of HAuCl$_4$ in the region around SiO$_2$ nanospheres than in the solution. Accordingly, after AA was introduced, the burst nucleation on Au seeds was occurred and led to the formation of a large number of Au nuclei around SiO$_2$ nanospheres. At a given reactant concentration of HAuCl$_4$, more nuclei with more nucleation sites imply insufficient Au source for forming long Au NWs. As a consequence, short Au nanoteeth other than long nanowires were formed after the localized seeded growth.

There are possibly two different seed-mediated growth mechanisms responsible for the formation of Au NWs and Au nanoteeth, as shown in **Figure 6**. Although in both cases Au seeds worked as active nucleation sites to initiate seeded anisotropic growth on SiO$_2$ nanospheres, the underlying growth mechanisms were totally different. For Au NWs through the diffusion growth approach, as discussed in the above paragraph, Au nuclei formed in the solution were diffused to and

nucleated at Au seeds on SiO$_2$ nanospheres, promoting the seeded growth of nanowires. During the whole growth process, Au seeds at one end of nanowires were immobilized on the surfaces of SiO$_2$ nanospheres, while the moving growth frontiers at another end were always pointed out to solution (Figure 6A). This is because the spatial positions of the growth frontier are easier accessible for Au nuclei diffusing from solution, compared with that of Au–SiO$_2$ interfaces at another end of the nanowires. For Au nanoteeth with the localized growth, the Au nuclei were mainly concentrated around the SiO$_2$@Au seeds (Figure 6B1). The high-concentration Au nuclei facilitated the nucleation and growth of nanowires at Au–SiO$_2$ interfaces. As a consequence, the favorable growth with growth frontiers always next to SiO$_2$ nanospheres was occurred, as shown in Figure 6B2. We noted that the same growth mechanism under similar experimental conditions (feeding order: HAuCl4+AA) had been reasonably explained, which was ascribed to the effect of ligand binding.[21] It is noteworthy that the new growth mechanism for the typical nanowires in this work is distinct from these for Au NW forest where the growth frontier always next to substrate[21] and well-known VLS growth where the growth frontier always next to catalyst.[38–42] Our proposition based on the diffusion growth and localized growth models provides a new perspective to fully and deeply understand the seed-mediated growth mechanism of Au NWs.

In addition, SiO$_2$ nanospheres and Au seeds are also key factors necessary for the preparation of Au NWs. As shown in Figure 4C, when the synthesis was conducted by direct reduction of HAuCl$_4$ using AA in the absence of the SiO$_2$@Au seed composites, only dispersed Au nanoparticles were obtained with the size of approximately 20 nm. To further investigate the independent effect of Au seeds, the SiO$_2$@Au seed composite solution was replaced by Au seed solution with other conditions being typical. It was found that Au nanoflowers consisting of several Au nanoparticles were generated in such a synthetic system without SiO$_2$ nanospheres (Figure 4D). Apparently, the nucleation of several Au nuclei on one Au seed and subsequent unlimited free growth of Au nuclei around Au seeds are
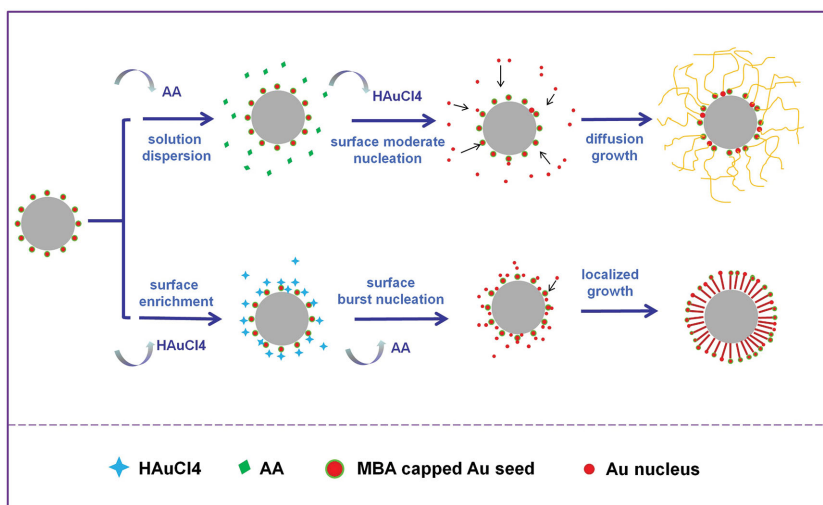
Figure 5. Schematic illustration of the proposed mechanism for the synthesis of SiO$_2$@Au composites.
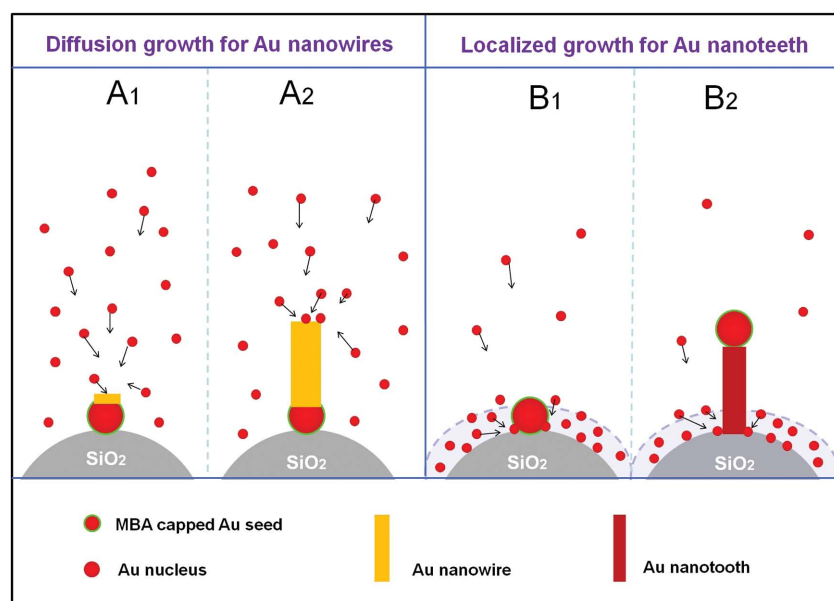
Figure 6. Schematic illustration of the proposed Au seed-mediated growth mechanisms for Au nanowires and nanoteeth.

the possible reason for the formation of these Au nanoflowers. Therefore, based on the data obtained above, the results can be briefly summarized here. i) Au seeds served as active and effective nucleation sites for the seeded growth of different Au nanostructures, namely Au NWs, nanoteeth, or nanoflowers, depending on the density of Au nucleation sites as well as whether employing SiO_2 nanospheres. ii) SiO_2 nanospheres provided highly curved substrates with limit space for the growth of radially arrayed 1D nanostructures such as Au NWs and nanoteeth. In this strategy, the preparation of the SiO_2@ Au seed composites with uniform and stable deposition of Au seeds is crucial for subsequent growth of 1D Au nanostructures. It is point out that the deposition of Au seeds and the growth of Au NWs on high-curvature surfaces of SiO_2 nanospheres make the strategy more challengeable.

The electrocatalytic activity of Au NWs was evaluated by cyclic voltammetry (CV) and amperometric methods. **Figure 7**A shows the CV responses of the Au NWs modified glassy carbon (GC) electrode in the presence ($2 \times 10^{-}$ M) and absence of H_2O_2 in 0.1 M phosphate buffer saline (PBS, pH 7.0) solution. After H_2O_2 was injected into the PBS solution, the reduction current increased greatly (Figure 7A, curve a), which was quite different from the system without H_2O_2 (Figure 7A, curve b). This result identifies the excellent catalytic performance of Au NWs towards to the reduction of H_2O_2.

This prominent catalytic activity was used to build the biosensor for the detection of H_2O_2 using chronoamperometry. The current–time (i–t) curves of different electrodes were compared under the same experimental conditions with successive additions of 0.5×10^{-3} M H_2O_2 into the stirred N_2-saturated 0.1 M PBS at −0.6 V. The typical Au NWs and Au nanoparticles were used to modify the GC electrodes (GCE), respectively, and their electrocatalytic activities towards the reduction of H_2O_2 were studied and compared with that of the GCE, as shown in Figure 7B. It is clear that the Au NWs/GCE displays the

highest current density response. Figure S4 (Supporting Information) shows the calibration lines of different electrodes based on reduction current response in the presence of H_2O_2. One can see that the slope and linear relationship of the Au NWs/GCE are higher than the others, demonstrating the higher sensitivity and stability for H_2O_2 detection.
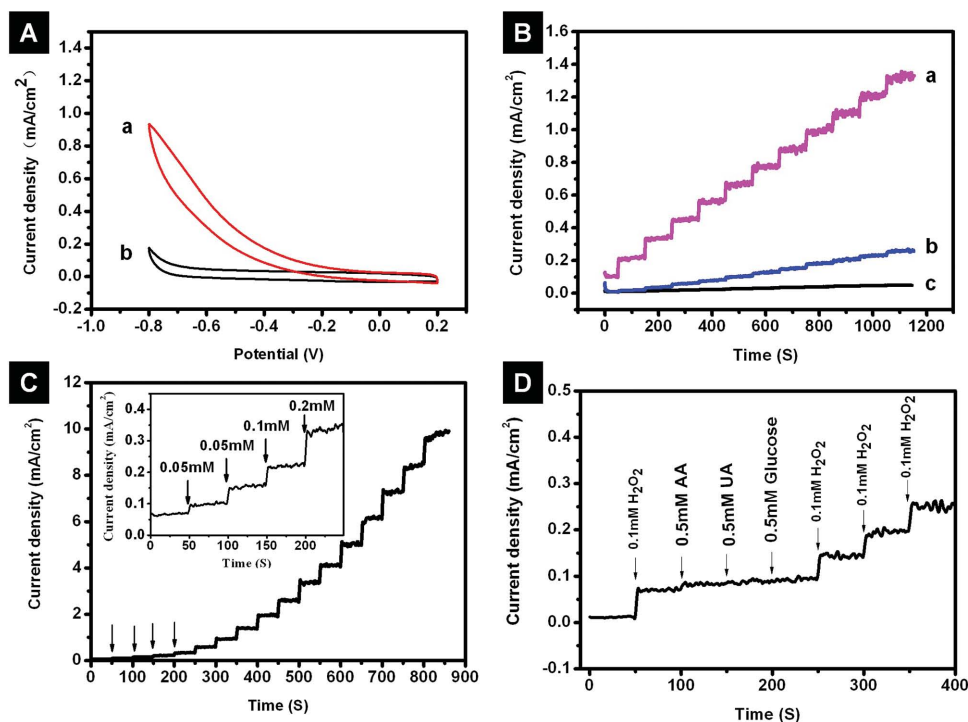
Figure 7C displays the typical amperometric responses of the Au NWs/GCE on successive injection of different concentrations of H_2O_2 into the stirred N_2-saturated PBS under the applied potential of −0.6 V. It is obvious that the continuous reduction current jumps and the current response increases rapidly to reach a steady-state value when H_2O_2 was successively added into the PBS solution. Figure S5 (Supporting Information) shows the calibration line with related parameters of Au NWs/GCE based on reduction current response in the presence of H_2O_2. The current response was proportional to the H_2O_2 concentration in the range of 0.05×10^{-3} to 22.65×10^{-3} M with a correlation coefficient of 0.99959. The detection limit was calculated to be 0.03×10^{-3} M ($S/N = 3$).

L-ascorbic acid, uric acid (UA), and glucose are the most commonly existing interference species in the physiological environment. The anti-interference effect of the sensor towards AA, UA, and glucose was evaluated in order to investigate the selectivity of the unique non-enzymatic sensor. Figure 7D reveals the amperometric responses of Au NWs/GCE upon successive addition of 0.1×10^{-3} M H_2O_2, 0.5×10^{-3} M UA, AA, and glucose, and 0.1×10^{-3} M H_2O_2 (three times) into N_2-saturated PBS solution (0.1 M, pH 7.0). The electrochemical signals responding to the four additions of H_2O_2 are basically identical. While the responses caused by high concentrations of UA, AA, and glucose could be negligible, suggesting a high selectivity of the Au NWs/GCE for H_2O_2 detection. In addition, the sensing performance towards H_2O_2 of the three electrodes was also tested in the presence of fetal bovine serum (FBS), as shown in Figure S6 (Supporting Information). FBS was added in the same order with a total volume up to 3 mL in each testing system. The response curves are not so regular relative to those obtained in pure buffer systems due possible to the existence of FBS. We can see that the Au NWs/GCE delivers the best performance among the three electrodes (Figure S6, Supporting Information). Therefore, it is expected that this novel Au NW-based non-enzymatic sensor can be introduced to the selective detection of H_2O_2 in the presence of these common physiological materials.

3. Conclusion

In summary, a novel strategy with the new growth mechanism for the large-scale fabrication of Au NWs has been developed, which involves controlled amine modification of SiO_2 nanospheres, Au seed loading on SiO_2 nanospheres, and subsequent seeded growth of Au NWs. The as-prepared Au

502 wileyonlinelibrary.com

© 2014 WILEY-VCH Verlag GmbH & Co. KGaA, Weinheim

Part. Part. Syst. Charact. **2015**, *32*, 498–504

Figure 7. A) CVs of the Au NWs/GCE in N_2 saturated 0.1 M PBS solution (pH 7.0) containing 2×10^{-3} M H_2O_2 (curve a) and 0×10^{-3} M (curve b). Scan rate: 50 mV s^{-1}. B) Steady-state current time responses of a) Au NWs/GCE, b) Au NPs/GCE, and c) GCE to the successive injection of 0.5×10^{-3} M H_2O_2 into stirred N_2-saturated PBS solution (0.1 M, pH 7.0) at -0.6 V vs SCE. C) Typical amperometric current responses of the Au NWs/GC electrode on successive addition of H_2O_2 (0.05×10^{-3}, 0.1×10^{-3}, 0.2×10^{-3}, 0.5×10^{-3}, 0.75×10^{-3}, 1.0×10^{-3}, 1.25×10^{-3}, 1.5×10^{-3}, 1.75×10^{-3}, 2.0×10^{-3}, 2.25×10^{-3}, 2.5×10^{-3}, 2.75×10^{-3}, 3.0×10^{-3} M) into stirred N_2-saturated PBS solution (0.1 M, pH 7.0) at -0.6 V vs SCE. Inset is the magnified current responses corresponding to the first four additions of H_2O_2. D) The current response of the Au NWs/GC electrode on addition of 0.1×10^{-3} M H_2O_2, 0.5×10^{-3} M (AA, UA, CA and glucose) into stirred N_2-saturated PBS solution (0.1 M, pH 7.0) at -0.6 V vs SCE.

NWs show long length, high aspect ratio, and good flexibility and can naturally form the dense and stable films. The new growth mechanism for the Au NWs has been proposed and discussed in comparison with that for Au nanoteeth and reported Au NW forest as well as well-known VLS growth. It is found that SiO_2 nanospheres and Au seeds, which offer high-curvature limited surface and mediate the seeded growth, respectively, are critical conditions for the formation of Au NWs, while the feeding order of the reactants (HAuCl$_4$ and AA) determines the final 1D Au structure and the related growth mechanisms. The Au NWs exhibit a prominent catalytic effect toward the reduction of H_2O_2 and have been used to develop nonenzymatic H_2O_2 sensor. The sensor exhibited advantages including fast response, wide linear range, good selectivity, long-term stability, and reproducibility. This demonstrates that Au NWs are expected to be a potential material for the nonenzymatic detection of H_2O_2. In addition, the synthetic strategy stressing the key factors of high-curvature substrate and seed-mediated growth for the preparation of long Au NWs and stable nanowire films may be applicable as a promising general method to other metal systems. These related investigations are under way.

4. Experimental Section

Materials: Tetraethylorthosilicate (TEOS), 3-aminopropyltriethoxysilane (APTES), MBA, UA, NaH$_2$PO$_4$, and Na$_2$HPO$_4$ were achieved from Aladdin. AA and NH$_3$.H$_2$O were purchased from Alfa Aesar. Sodium Citrate was obtained from Sigma–Aldrich. The other reagents were achieved from Beijing Sinopharm Chemical Reagents Company (Beijing, China). All of the reagents were of analytical grade and used as received. Water used for solution preparation was deionized (resistivity >18 MΩ cm).

Deposition of Au Nanoseeds on SiO$_2$ Nanospheres (SiO$_2$@Au seeds): First, silica nanospheres ($d = 220$ nm) were synthesized by the Störber method[46] and used as curved substrate for Au seed deposition and nanowire growth. To ensure effective and stable Au seed deposition, the surfaces of spheres were functionalized with amino groups using APTES before use. The gold seeds ($d = 8$ nm) were prepared by the reduction of HAuCl$_4$ (0.3×10^{-3} M) using borohydride (0.2×10^{-3} M) in the presence of sodium citrate (1.0×10^{-3} M).[47] To prepared SiO$_2$@Au seed composites, 1 mL of 12 mg L^{-1} aminated SiO$_2$ nanospheres was dispersed in 20 mL ethanol, followed by the dropwise addition of 60 mL Au seed solution. After stirring for 12 h, the composites were centrifuged at 8500 rpm, washed for three times, and stocked in 25 mL water.

Growth of Long Au NWs on SiO$_2$ Nanospheres (SiO$_2$@Au NWs): The SiO$_2$@Au seed composites were dispersed in a water–ethanol (3:1, v/v) mixed solution. Then, 0.66 mL of 10×10^{-3} M MBA was added with stirring. Subsequently, 0.1 mL of 0.492 M AA and 0.405 mL of 50×10^{-3} M chloroauric acid (HAuCl$_4$) were added in turn. After 15 min, the product was collected using the centrifuge method, washed by ethanol for one time and by water for three times. Au NW film was prepared after readily removing silica nanospheres by NaOH solution.

Characterization: The morphology was characterized using a SEM (Hitachi S4800, 3 kV) and HRTEM (JEM 2011, 200 kV). The UV–vis spectra of the samples were recorded on a UV–vis spectrometer (Varian Cary 500). The crystal structure was determined by XRD using a D/max2550VB3+/PC X-ray diffractometer with Cu Ka radiation with a

Particle
& Particle Systems Characterization

www.particle-journal.com

www.MaterialsViews.com

Materials Views

FULL PAPER

1.5418 °A wavelength. A beam voltage of 40 kV and a 100 mA current beam were used. The electrochemical measurements were carried out on a CHI 660E (Chenhua, China) at room temperature. A saturated calomel electrode (SCE) was used as the reference electrode for all the electrochemical tests. A Pt electrode was used as the counter electrode and a GC or Au NWs (or Au NPs)-modified GC electrode was used as the working electrode. The nitrogen-saturated 0.1 M PBS was used as the supporting electrolyte during the measurement of H_2O_2.

Preparation of Au NW/GC and Au NP/GC Electrode: The GC electrode was carefully polished with 0.05 μm alumina powder, followed by successive sonication in ethanol and water for 5 min, and dried in the air. Then, the GC electrode was tested in 0.5×10^{-3} M $K_3Fe(CN)_6$/0.2 M KCl solution by cycling its potential between −0.2 and 0.6 V (vs SCE). While the electric potential difference was between 65 and 85 mV, the GC electrode was washed with water and reserved. Then, 10 μL of the condensed Au NWs (or Au NPs) solution was dropped onto the GC electrode and dried in an oven at 55 °C for 10 min. Finally, 10 μL of 0.05 wt% Nafion (Aldrich) was dropped onto the modified electrode to form a protective layer. The prepared electrode was defined as GC/Au NWs (or GC/Au NPs).

Supporting Information

Supporting Information is available from the Wiley Online Library or from the author.

Acknowledgements

[1] B. Peng, G. Y. Li, D. H. Li, S. Dodson, Q. Zhang, J. Zhang, Y. H. Lee, H. V. Demir, X. Y. Ling, Q. H. Xiong, *ACS Nano* **2013**, *7*, 5993.

[2] L. Dykmana, N. Khlebtsov, *Chem. Soc. Rev.* **2012**, *41*, 2256.

[3] J. C. Y. Kah, C. Grabinski, E. Untener, C. Garrett, J. Chen, D. Zhu, S. M. Hussain, K. Hamad-Schifferli, *ACS Nano* **2014**, *8*, 4608.

[4] S. E. Lee, D. Y. Sasaki, Y. Park, R. Xu, J. S. Brennan, M. J. Bissell, L. P. Lee, *ACS Nano* **2012**, *6*, 7770.

[5] K. D. Osberg, M. Rycenga, N. Harris, A. L. Schmucker, M. R. Langille, G. C. Schatz, C. A. Mirkin, *Nano Lett.* **2012**, *12*, 3828.

[6] L. G. Xu, Y. Liu, Z. Y. Chen, W. Li, Y. Liu, L. M. Wang, Y. Liu, X. C. Wu, Y. L. Ji, Y. L. Zhao, L. Y. Ma, Y. M. Shao, C. Y. Chen, *Nano Lett.* **2012**, *12*, 2003.

[7] N. R. Jana, L. Gearheart, C. J. Murphy, *J. Phys. Chem. B* **2001**, *105*, 4065.

[8] S. T. Sivapalan, B. M. DeVetter, T. K. Yang, T. van Dijk, M. V. Schulmerich, P. S. Carney, R. Bhargava, C. J. Murphy, *ACS Nano* **2013**, *7*, 2099.

[9] C. J. Murphy, T. K. San, A. M. Gole, C. J. Orendorff, J. X. Gao, L. Gou, S. E. Hunyadi, T. Li, *J. Phys. Chem. B* **2005**, *109*, 13857.

[10] S. E. Lohse, C. J. Murphy, *Chem. Mater.* **2013**, *25*, 1250.

[11] A. Kisner, M. Heggen, E. Fernandez, S. Lenk, D. Mayer, U. Simon, A. Offenhausser, Y. Mourzina, *Chem. Eur. J.* **2011**, *17*, 9503.

[12] A. Sanchez-Iglesias, B. Rivas-Murias, M. Grzelczak, J. Perez-Juste, L. M. Liz-Marzan, F. Rivadulla, M. A. Correa-Duarte, *Nano Lett.* **2012**, *12*, 6066.

[13] C. Wang, Y. J. Hu, C. M. Lieber, S. H. Sun, *J. Am. Chem. Soc.* **2008**, *130*, 8902.

[14] C. H. Moon, M. L. Zhang, N. V. Myung, E. D. Haberer, *Nanotechnology* **2014**, *25*.

[15] M. Jung, H. Noh, Y.-J. Doh, W. Song, Y. Chong, M.-S. Choi, Y. Yoo, K. Seo, N. Kim, B.-C. Woo, B. Kim, J. Kim, *ACS Nano* **2011**, *5*, 2271.

[16] Y. Kanno, T. Suzuki, Y. Yamauchi, K. Kuroda, *J. Phys. Chem. C* **2012**, *116*, 24672.

[17] X. Y. Zhang, L. D. Zhang, Y. Lei, L. X. Zhao, Y. Q. Mao, *J. Mater. Chem.* **2001**, *11*, 1732.

[18] S. Meltzer, R. Resch, B. E. Koel, M. E. Thompson, A. Madhukar, A. A. G. Requicha, P. Will, *Langmuir* **2001**, *17*, 1713.

[19] A. Halder, N. Ravishankar, *Adv. Mater.* **2007**, *19*, 1854.

[20] C. Zhu, H.-C. Peng, J. Zeng, J. Y. Liu, Z. Gu, Y. N. Xia, *J. Am. Chem. Soc.* **2012**, *134*, 20234.

[21] J. T. He, Y. W. Wang, Y. H. Feng, X. Y. Qi, Z. Y. Zeng, Q. Liu, W. S. Teo, C. L. Gan, H. Zhang, H. Y. Chen, *ACS Nano* **2013**, *7*, 2733.

[22] C. Yang, H. W. Gu, W. Lin, M. M. Yuen, C. P. Wong, M. Y. Xiong, B. Gao, *Adv. Mater.* **2011**, *23*, 3052.

[23] L. B. Hu, H. S. Kim, J.-Y. Lee, P. Peumans, Y. Cui, *ACS Nano* **2010**, *4*, 2955.

[24] J.-Y. Lee, S. T. Connor, Y. Cui, P. Peumans, *Nano Lett.* **2008**, *8*, 689.

[25] F. Antunes, E. Cadenas, *Free Radical Biol. Med.* **2001**, *30*, 1008.

[26] M. P. Gimeno, M. C. Mayoral, J. M. Andres, *Anal. Methods* **2013**, *5*, 1510.

[27] N. V. Klassen, D. Marchington, H. C. E. McGowan, *Anal. Chem.* **1994**, *66*, 2921.

[28] A. Lobnik, M. Cajlakovic, *Sens. Actuators, B* **2001**, *74*, 194.

[29] S. M. Steinberg, *Monit. Assess.* **2013**, *185*, 3749.

[30] J. C. Yuan, A. M. Shiller, *Anal. Chem.* **1999**, *71*, 1975.

[31] L. S. Zhang, G. T. F. Wong, *Talanta* **1999**, *48*, 1031.

[32] A. I. Gopalan, S. Komathi, G. S. Anand, K.-P. Lee, *Bioelectronics* **2013**, *46*, 136.

[33] S. Komathi, A. I. Gopalan, S.-K. Kim, G. S. Anand, K.-P. Lee, *Electrochim. Acta* **2013**, *92*, 71.

[34] E. Koposova, X. Liu, A. Kisner, Y. Ermolenko, G. Shumilova, A. Offenhaeusser, Y. Mourzina, *Biosens. Bioelectron.* **2014**, *57*, 54.

[35] X. Zhao, Z. Mai, X. Kang, X. Zou, *Biosens. Bioelectron.* **2008**, *23*, 1032.

[36] Y. Chen, P. Gai, L. Jin, D. Zhu, D. Tian, E. S. Abdel-Halim, J. Zhang, J.-J. Zhu, *J. Mater. Chem. B* **2013**, *1*, 3451.

[37] H. Fan, S. Zhang, P. Ju, H. Su, S. Ai, *Electrochim. Acta* **2012**, *64*, 171.

[38] M. Law, J. Goldberger, P. D. Yang, *Annu. Rev. Mater. Res.* **2004**, *34*, 83.

[39] P. X. Gao, Y. Ding, W. J. Mai, W. L. Hughes, C. S. Lao, Z. L. Wang, *Science* **2005**, *309*, 1700.

[40] X. J. Wang, G. P. Li, T. Chen, M. X. Yang, Z. Zhang, T. Wu, H. Y. Chen, *Nano Lett.* **2008**, *8*, 2643.

[41] Z. Zhang, L. M. Wong, H. G. Ong, X. J. Wang, J. L. Wang, S. J. Wang, H. Chen, T. Wu, *Nano Lett.* **2008**, *8*, 3205.

[42] Y. Y. Wu, H. Q. Yan, M. Huang, B. Messer, J. H. Song, P. D. Yang, *Chem. Eur. J.* **2002**, *8*, 1261.

[43] W. L. Barnes, A. Dereux, T. W. Ebbesen, *Nature* **2003**, *424*, 824.

[44] J. Ye, P. van Dorpe, *Nanoscale* **2012**, *4*, 7205.

[45] H. T. Sun, X. Sun, M. P. Yu, A. K. Mishra, L. P Huang, J. Lian, *Adv. Funct. Mater.* **2014**, *24*, 2389.

[46] W. Stöber, A. Fink, E. Bohn, *J. Colloid Interface Sci.* **1968**, *26*, 62.

[47] K. R. Brown, D. G. Walter, M. J. Natan, *Chem. Mater.* **2000**, *12*, 306.